Available online at www.sciencedirect.com
SCIENCE DIRECT®
Coordination Chemistry Reviews 249 (2005) 1460–1467
COORDINATION CHEMISTRY REVIEWS
www.elsevier.com/locate/ccr

Review

Synthesis of novel ruthenium sensitizers and their application in dye-sensitized solar cells

Md. K. Nazeeruddin *, C. Klein, P. Liska, M. Grätzel **

Laboratory for Photonics and Interfaces, Institute of Chemical Sciences and Engineering, School of Basic Sciences, Swiss Federal Institute of Technology, CH-1015 Lausanne, Switzerland

Received 14 February 2005
Available online 18 April 2005

Contents

Abstract

Ruthenium(II) complexes $[Ru(L_2)(NCS)_2]$ (K8) and $[Ru(L)(L^9)(NCS)_2]$ (K9) (where L = 4,4′-bis(carboxyvinyl)-2,2′-bipyridine and L^9 = 4,4′-dinonyl-2,2′-bipyridine) were synthesized and characterized by spectroscopic and electrochemical techniques. The performance of K8 and K9 complexes as charge transfer photosensitizers in nanocrystalline TiO_2 based solar cells was investigated. These complexes when anchored onto TiO_2 films exhibit very efficient sensitization yielding $75 \pm 5\%$ incident photon-to-current efficiencies (IPCE) in the visible region using an electrolyte consisting of 0.6 M methyl-*N*-butyl imidazolium iodide, 0.05 M iodine, 0.1 M LiI and 0.5 M *tert*-butylpyridine in 50/50 (v/v) mixture of valeronitrile and acetonitrile. At one sun the K8 complex gave a short circuit photocurrent density of 18 ± 0.5 mA/cm^2, the open circuit voltage 640 ± 50 mV and fill factor of 0.75 ± 0.05, corresponding to an overall conversion efficiency of $8.64 \pm 0.5\%$. Under

* Corresponding author. Fax: +41 21 693 4111.
** Co-Corresponding author.
E-mail address: MdKhaja.Nazeeruddin@epfl.ch (Md.K. Nazeeruddin).

0010-8545/$ – see front matter
doi:10.1016/j.ccr.2005.03.025

similar conditions, the K9-sensitized solar cell gave a photocurrent density of 16.5 ± 0.5 mA/cm^2, 666 ± 50 mV open circuit potential and 0.71 ± 0.05 fill factor yielding $7.81\% \pm 0.6\%$ efficiency.

Keywords: Ruthenium(II) sensitizers; Hydrophobic heteroleptic ruthenium complexes; Dye-sensitized solar cells; Photovoltaic cells; Nanocrystalline TiO_2 films; Solar energy conversion

1. Introduction

Dye-sensitized solar cells are currently attracting widespread interest for the conversion of sunlight into electricity because of their low cost and high efficiency [1–7]. In these cells, dye is one of the key components for high power conversion efficiencies. The pioneering studies on dye-sensitized nanocrystalline TiO_2 films using *cis*-dithiocyanatobis(4,4′-dicarboxylic acid-2,2′-bipyridine)Ruthenium(II), (N3) is a paradigm in this field. In spite of this, the main drawback of this sensitizer is the lack of absorption in the red region of the visible spectrum and also relatively low molar extinction coefficient [8]. Many researchers have tried to overcome these shortcomings without significant success [9–12]. The molecular engineering of ruthenium complexes for TiO_2-based solar cells presents a challenging task as several stringent requirements have to be fulfilled by the sensitizer and these are very difficult to be met simultaneously, including absorption of all the visible light and function as an efficient charge transfer sensitizer. For example, the lowest unoccupied molecular orbitals (LUMO) and the highest occupied molecular orbitals (HOMO) have to be maintained at levels where photo-induced electron transfer into the TiO_2 conduction band and regeneration of the dye by iodide can take place at practically 100% yield. We report here a study in which we have maintained these conditions and at the same time have succeeded in fine-tuning the spectral properties of ruthenium polypyridyl complexes by designing at molecular level a novel ligand 4,4′-bis(carboxyvinyl)-2,2′-bipyridine. Our research focused on increasing the optical extinction coefficient of sensitizers, so that dye solar cells could be made thinner and thus more efficient because of reduced transport losses in the nanoporous environment. In this article, we report the synthesis and characterization of ruthenium sensitizers using our new ligand and their application in dye-sensitized solar cell.

2. Experimental

2.1. Materials

The solvents and reagents puriss grade quality were purchased from Fluka. 4,4′-dinonyl-2,2′-bipyridine (dnbpy), dichloro(*p*-cymene)ruthenium(II) dimer and potassium/ammonium thiocyanate were obtained (from Aldrich) and used as received. LH-20 Sephadex gel was obtained from Pharmacia. The intermediate product 4,4′-diformyl-2,2′-bipyridine, 4,4′-bis(carboxyvinyl)-2,2′-bipyridine ligand and its homoleptic ruthenium complex (K8) were synthesized according to literature procedures [13,14]. Tetrahydrofuran (THF) and toluene were distilled over sodium and under argon.

2.2. Analytical measurements

UV–vis and fluorescence spectra were recorded in 1 cm path length quartz cell on a Cary 5 spectrophotometer and Spex Fluorolog 112 Spectrofluorimeter, respectively. Electrochemical data were obtained by cyclic voltammetry in a conventional three-electrode cell with a PAR potentiostat. A glassy-carbon or a gold working electrode, platinum-wire auxiliary electrode and saturated silver chloride electrodes were used in a single-compartment-cell configuration. ^{1}H and ^{13}C NMR spectra were measured on a Bruker 200 MHz spectrometer. The reported chemical shifts were in ppm against TMS. The ATR-FTIR spectra for all the samples were measured using a Digilab 7000 FTIR spectrometer. The ATR data reported here were taken with the 'Golden Gate' diamond anvil ATR accessory (Graseby–Specac) typically using 64 scans at a resolution of 2 cm^{-1}. The IR optical bench was flushed with dry air.

2.3. TiO_2 electrode preparation

TiO_2 anatase nanoparticles of 16 nm were prepared by hydrolysis of titanium(IV)isopropoxide as described before [15]. The nanocrystalline TiO_2 thin films of 12 μm thick were deposited onto transparent conducting glass (TEC-15, USA which has been coated with a fluorine-doped stannic oxide layer, sheet resistance of 12–15 Ω/cm^2, by screen-printing). These films were dried at 150 °C for 20 min and then a 4 μm thick layer of 400 nm TiO_2 particles (400 nm particles were obtained from CCI, Japan) was deposited again using a screen-printing method. The double-layered films were sintered at 500 °C for 20 min.

The heated electrodes were impregnated with a 0.05 M titanium tetrachloride solution in a water saturated desiccator for 30 min at 70 °C and washed with distilled water. The 0.05 M titanium tetrachloride solution was prepared in the following manner: first, 2 M titanium tetrachloride solution was prepared by adding directly titanium tetrachloride liquid into a bottle containing ice, which was cooled to −20 °C, then the solution was further diluted to 0.05 M. Finally, the electrodes were heated at 520 °C for 20 min and allowed to cool to 50 °C before dipping into the dye solution.

Dye solutions were prepared in the concentration range of $3–5 \times 10^{-4}$ M in 1:1 (v/v) acetonitrile and *tert*-butanol solution and the electrodes were dipped into it for 18–22 h. The dye-coated electrodes were rinsed quickly with acetonitrile and used as such for photovoltaic measurements.

2.4. Dye-sensitized solar cell fabrication

The dye deposited film is used as a working electrode. A sandwich cell was prepared with a second conducting glass coated with chemically deposited platinum from 0.05 M hexachloroplatinic acid. The platinum coated counter electrode and the dye-coated TiO_2 film were then put together with a thin transparent film of Surlyn polymer frame (DuPont). The sandwiched electrodes were tightly held and then heat (130 °C) applied around the Surlyn frame to seal the two electrodes. A thin layer of electrolyte consisting of 0.6 M *N*-methyl-*N*-butyl imidazolium (BMII); 0.05 M I_2; 0.1 M LiI; 0.5 M *tert*-butyl pyridine in 1:1 acetonitrile + valeronitrile (1376 from now on) was introduced into inter electrode space from the counter electrode side through pre-drilled holes. The drilled holes were sealed with microscope cover slide and Surlyn to avoid leakage of the electrolyte solution.

2.5. Photoelectrochemical measurements

Photoelectrochemical data were measured using a 450 W xenon light source that was focused to give 1000 W/m^2, the equivalent of one sun at air mass 1.5, at the surface of the test cell. The spectral output of the lamp was matched in the region of 350–750 nm with the aid of a Schott KG-5 sunlight filter so as to reduce the mismatch between the simulated and the true solar spectrum to less than 2%. The differing intensities were regulated with neutral wire mesh attenuators. The applied potential and measured cell current were measured using a Keithley Model 2400 digital source meter. The current–voltage characteristics of the cell under these conditions were determined by biasing the cell externally and measuring the generated photocurrent. This process was fully automated using Wavemetrics software. A similar data acquisition system was used to control the incident photon-to-current conversion efficiency (IPCE) measurement. Under full computer control, light from a 300 W Xe lamp was focused through a high throughput monochromator onto the photovoltaic cell under test. The monochromator was incremented through the visible spectrum to generate the IPCE (λ) curve as defined below,

$$\mathrm{IPCE}(\lambda) = 1240 \left(\frac{I_{sc}}{\lambda \phi} \right)$$

where λ is the wavelength, I_{sc} the current at short circuit (mA/cm^2) and ϕ is the incident radiative flux (W/m^2). The photoelectrochemical properties were investigated by measuring the current and voltage (*I–V*) characteristics.

3. Syntheses and characterization

3.1. Synthesis of [Ru(II)LL^9 (NCS)$_2$], K9 complex

A mixture of 4,4′-dinonyl-2,2′-bipyridine (150 mg, 0.37 mmol) and dichloro(*p*-cymene)ruthenium(II) dimer (113 mg, 0.18 mmol) in argon degassed absolute ethanol (40 mL) was heated to reflux for 4 h. Evaporation of the solvent leaded to dichloro(*p*-cymene)-4,4′-dinonyl-2,2′-bipyridine–ruthenium(II) complex as a brown-yellow oil. This intermediate complex was used without further purification.

A mixture of dichloro(*p*-cymene)–4,4′-dinonyl-2,2′-bipyridine–ruthenium(II) complex (255 mg, 0.36 mmol) and 4,4′-bis(carboxyvinyl)-2,2′-bipyridine (106 mg, 0.36 mmol) in dry and argon degassed DMF (30 mL) was heated to 150 °C for 4 h. To the resulting dark purple solution was added NH_4NCS (408 mg, 5.4 mmol) and the resulting mixture was heated to 150 °C for 4 h more. After evaporation of the DMF, the resulting purple residue was suspended in water (200 mL) and sonicated for 5 min. The pH was adjusted to 3 with HNO_3 (0.02 M) and the mixture was let stand in the fridge overnight.

The reaction flask was allowed to warm to 25 °C and the solution was filtered through a G4 sintered glass crucible by suction filtration. The solid was further washed with distilled water and diethyl ether and obtained as a dark powder. Yield (190 mg) 65%. The NMR spectra show presence of ≅15% S-bonded isomers, which were reduced to ≅3% by passing through a Sephadex LH-20 column three times using the following procedure.

The crude complex was dissolved in methanol containing two equivalents of tetrabutylammonium hydroxide. The concentrated solution was filtered through a sintered glass crucible and charged onto a LH-20 Sephadex column, which was prepared in methanol. The adsorbed complex was eluted using methanol as an eluent. The main band was collected and the solution pH was lowered to 3 using 0.02 M HNO_3 acid. The precipitated complex was collected on a glass frit and air-dried. Yield (60 mg) 32%.

^{1}H NMR (δ_H (ppm) in DMSO-d$_6$, *J* Hz): 9.21 (d, H^{6,5}, *J* 5.9); 9.13 (s, H′^{3}); 9.07 (d, H$^{6',5'}$, *J* 5.9); 8.98 (s, H$^{3'}$); 8.67 (s, H$^{3''}$); 8.52 (s, H$^{3'''}$); 8.09 (d, H^{5,6}, *J* 5.8); 7.81 (d, H$^{5',6'}$, *J* 5.9); 7.66 (d, vinyl-H, *J* 15.94); 7.51 (d, H$^{6'',5''}$, *J* 5.98); 7.38 (d, H$^{6''',5'''}$, *J* 5.88); 7.37 (d, vinyl-2H, *J* 16.05); 7.14 (d, H$^{5'',6''}$, *J* 5.8); 7.10 (d, vinyl-H, *J* 15.94); 7.09 (d, H$^{5''',6'''}$, *J* 5.6); 2.91 (t, 2H), 2.65(t, 2H), 1.91 (m, 2H), 1.57 (m, 26H), 0.81 (t, 6H).

^{13}C NMR 200 MHz, (DMSO-d$_6$) δ ppm: 168.07 (C^9); 168.01 (C$^{9'}$); 159.25 (C^2); 158.07 (C$^{2'}$); 157.94 (C$^{2''}$); 156.86 (C$^{2'''}$); 152.75 (C^6); 152.01 (C$^{6'}$); 151.85 (C$^{6''}$); 151.29 (C$^{6'''}$); 153.09 (C^4); 152.51 (C$^{4'}$); 142.79 (C$^{4''}$); 142.15 (C$^{4'''}$); 137.84 (C^8); 137.14 (C$^{8'}$); 134.17 (C of NCS); 133.59 (C of NCS′); 129.55 (C^7); 128.85 (C$^{7'}$); 125.35 (C^3); 126.68 (C$^{3'}$); 125.74 (C$^{3''}$); 125.05 (C$^{3'''}$); 123.81 (C^5); 123.78 (C$^{5'}$); 121.07 (C$^{5''}$); 120.71 (C$^{5'''}$).

Aliphatic carbons: 38.14 (–C_1); 37.73 (–$C_{1'}$); 35.01 (–C_2); 34.63 (–$C_{2'}$); 31.63 (–C_3); 31.53 (–$C_{3'}$); 30.17 (–C_4); 29.94 (–$C_{4'}$); 29.30 (–$C_{5,6}$); 29.19 (–$C_{5',6'}$); 29.02 (–$C_{7,8}$); 28.92 (–$C_{7',8'}$); 22.45 (–C_9); 22.39 (–$C_{9'}$).

4. Results and discussion

4.1. Synthetic studies

Fig. 1 shows the structures of the 4,4′-bis(carboxyvinyl)-2,2′-bipyridine ligand as its ruthenium complex [Ru(II)L_2(NCS)$_2$] K8, which has been reported previously [14] and the K9, whose synthesis is described here. The ligand 4,4′-bis(carboxyvinyl)-2,2′-bipyridine is synthesized in two steps [14] and its ruthenium complexes in a one pot synthesis starting from dichloro(*p*-cymene)ruthenium(II) dimer in DMF. The proton NMR spectra of the crude complexes show peaks at lower field, due to linkage isomers. Both the complexes contain the thiocyanate ligand, which is an ambidentate ligand which can coordinate to the ruthenium center through the –N or –S end, producing a mixture of isomers (≅85% N-bonded, and ≅15% S-bonded). Several attempts to remove S-bonded linkage isomers using re-crystallization procedure have failed. However, repeated purification of both complexes (three times) on a Sephadex LH-20 column yielded significantly enriched N-bonded isomers (≅97% N-bonded). The spectroscopic data of these complexes are consistent with structures shown in Fig. 1.

4.2. Absorption spectra

Fig. 2a show absorption spectra of the K8 and K9 complexes measured in *N*,*N*′-dimethylformamide (DMF) solu-

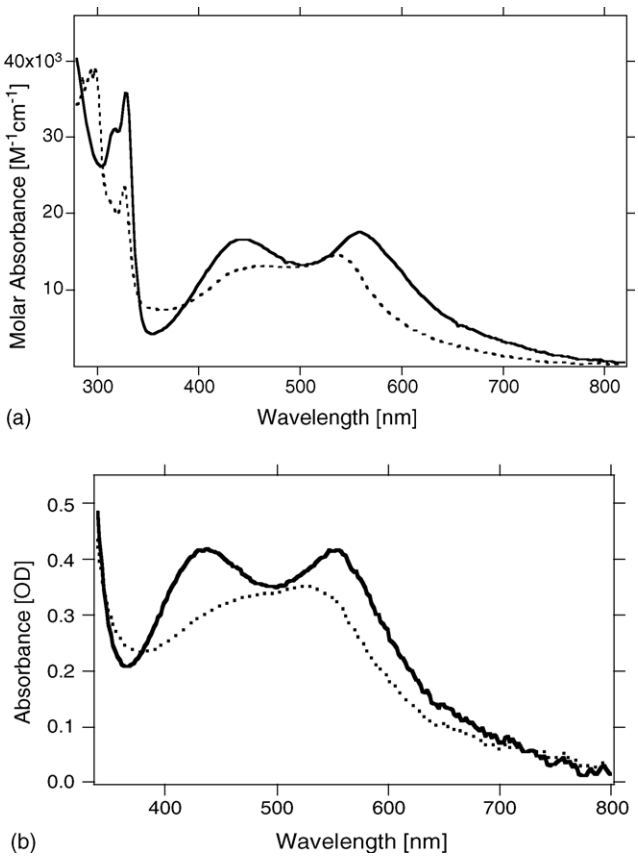

Fig. 2. (a) UV–vis absorption spectra of K8 (solid line) and K9 (dotted line) complexes measured in DMF and (b) a portion of the UV–vis absorption spectra of K8 (solid line) and K9 (dotted line) complexes adsorbed on to a nanocrystalline 2 μm thick transparent TiO_2 film; a similar 2 μm thick TiO_2 nanocrystalline film was used as blank. The data below 330 nm are not useful because of absorption by the conducting glass.

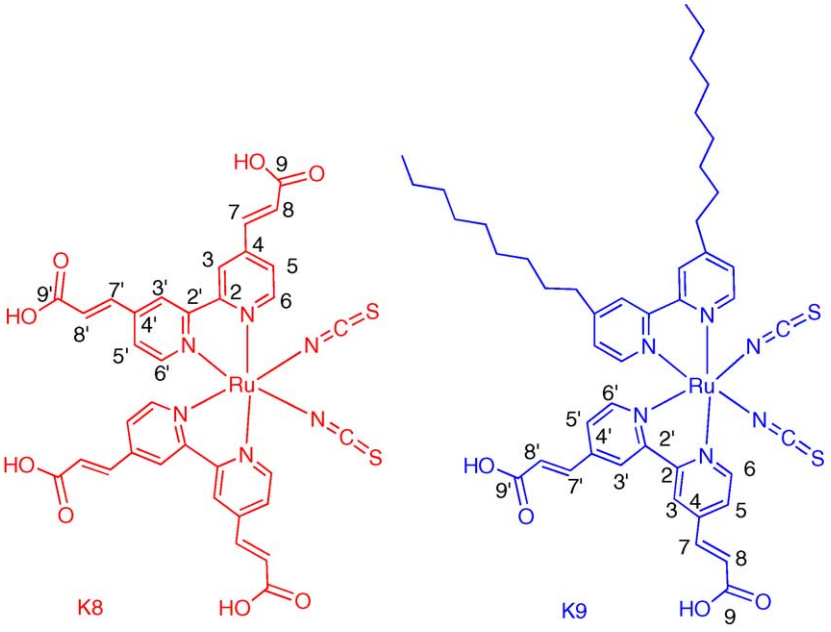

Fig. 1. Chemical structures of K8 and K9 complexes and the numbering scheme show our tentative assignments for NMR peaks.

tion. The K8 and K9 complexes show broad and intense absorption bands between 370 and 570 nm, due to metal-to-ligand charge transfer transitions (MLCT) [16]. The K9 complex, in DMF solution shows maxima at 534 nm (Fig. 2a), which is blue shifted by 22 nm compared to the K8 complex (λ_{max} 556 nm) [14]. In the UV region the K9 complex shows two distinct intra ligand (π–π^*) charge transfer transitions at 326 and 298 nm that are assigned to 4,4′-bis(carboxyvinyl)-2,2′-bipyridine and 4,4′-dinonyl-2,2′-bipyridine ligands, respectively [17]. The molar extinction coefficient of the lowest energy MLCT band in the K9 complex is 14500 M^{-1} cm^{-1}, which is ≈20% lower than the K8 complex (λ_{max} 556 nm and ε 17400 M^{-1} cm^{-1}) due to substitution of 4,4′-bis(carboxyvinyl)-2,2′-bipyridine by 4,4′-dinonyl-2,2′-bipyridine [14]. When the K8 and K9 complexes are excited within the MLCT absorption band at 298 K in an air-equilibrated DMF solution, they exhibit luminescence maxima at 830 and 795 nm, respectively. The blue shift of the emission maxima of the K9 complex compared to the K8 complex is coherent with blue shifted absorption spectrum of the K9 complex.

The absorption spectra of the two complexes adsorbed onto a 2 μm thick TiO_2 nanocrystalline film (photo anode electrode) are shown in Fig. 2b. The low energy MLCT maximum in the K9 complex is broad and slightly blue shifted upon adsorption onto TiO_2 nanocrystalline electrode compared to the solution spectrum. This is due to the fact that on the electrode the carboxylic acid groups bind to the TiO_2 surface by liberating protons causing an increase in the LUMO levels of the anchoring ligand (ATR-FTIR data, discussed below are consistent with dissociation of protons). The positions of the two MLCT bands of K8 complex adsorbed onto TiO_2 nanocrystalline film (436 and 556 nm) and in solution are very similar because of the presence of two 4,4′-bis(carboxyvinyl)-2,2′-bipyridine ligands in which all the carboxylic acid groups are not anchored. The K8 complex low energy MLCT maxima is red shifted by 22 nm compared to the K9 anchored complex consistent with the solution absorption spectra, which is also reflected in the IPCE spectra.

4.3. NMR spectral data

The ^1H and ^{13}C NMR spectra of K9 complex are consistent with the structure shown in Fig. 1, which are complicated because of the presence of two types of 2,2-bipyridine ligands in which all the pyridyl rings are electronically in different environment. Fig. 3 shows a comparison of portion of ^1H NMR spectra of the K8 and K9 complexes. The presence of 14 peaks, in the K9 complex which integrate for the presence of 16 protons indicate that the complex is not a mixture of 1:1 homoleptic complexes. The proton coupling constant data of the vinyl protons 15.94 and 16.04 Hz confirm that they are in a *trans* configuration.

Fig. 4 shows a comparison ^{13}C NMR spectra of the K8 and K9 complexes in the aromatic region between δ 170 and 120 ppm. The K9 complex exhibits 28 resonance signals corresponding to the 28 chemically dissimilar carbon atoms. In the K9 complex, two halves of each bipyridine ligand are in distinct magnetic environments and show 26 resonance peaks in the aromatic region due to four pyridyl rings and vinyl carbons. The two NCS ligands are *trans* to two different pyridyl rings; therefore, the electronic density of the two NCS ligands is not equivalent and separate resonance peaks are observed. The peaks at 168.07 (C^9) and 168.01 ($C^{9'}$) are due to the two carboxylic acid groups, which are *trans* to NCS and *trans* to pyridyl unit. A set of four peaks between 159.25 and 156.86 ppm is assigned to four C2, C2′, C2″ and C2‴ carbons. The second set of four resonance signals between 153 and 151 is assigned to the C6, C6′, C6″ and C6‴. The two peaks at 153.09 and 152.51, are assigned

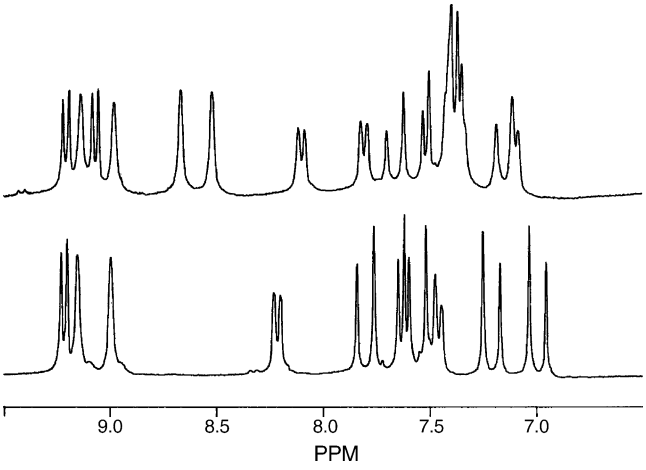

Fig. 3. A part of proton NMR spectra of the K8 (bottom trace) and K9 (top trace) complexes in DMSO-d_6. For clarity the peaks in the aliphatic region are not included.

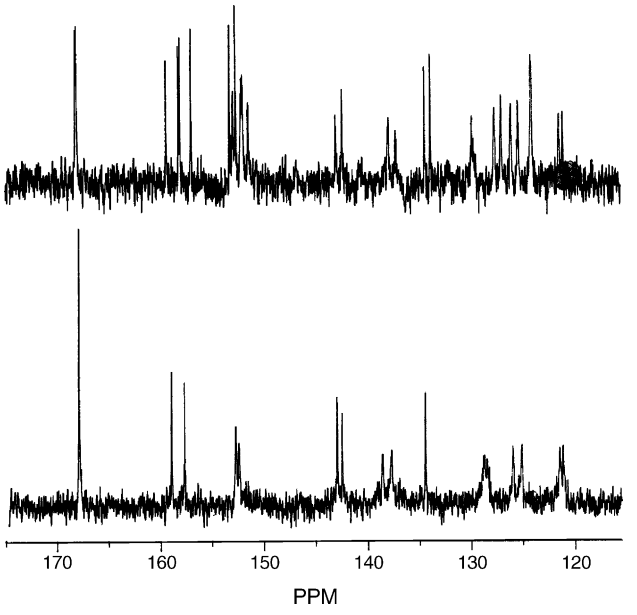

Fig. 4. A part of ^{13}C NMR spectra of the (bottom trace) and K9 (top trace) complexes in DMSO-d_6. For clarity the peaks in the aliphatic region are not included.

to the C4 and C4′ of 4,4′-bis(carboxyvinyl)-2,2′-bipyridine. The peaks at 139.27 and 138.56 were assigned to C4 and C4′ of 4,4′-dinonyl-2,2′-bipyridine. The eight resonance peaks between 125 and 120 ppm are due to C3 and C5 carbons and no attempts were made to identify individual carbons [18]. The peaks at 137.84, 137.14, 129.55 and 128.85 are assigned to the vinyl carbons, which are next to the carboxylic acid group and to the pyridine rings, respectively. The peaks at 134.17 and 133.59 ppm are due to two NCS ligands, which are *trans* to the 4,4′-bis(carboxyvinyl)-2,2′-bipyridine ring and the other one is *trans* to 4,4′-dinonyl-2,2′-bipyridine, respectively. Carbon-13 NMR spectra of complexes containing NCS ligands are useful to identify their mode of coordination. The N-coordinated thiocyanate carbon resonance peak has been reported in number of complexes at 130–135 ppm [19]. The presence of peaks in K9 complex in 130–135 ppm region indicate that NCS ligands are coordinated through the nitrogen end [20].

There is an inequality in the electron density on the two nonyl chains of the 2,2′-bipyridine, in which one is *trans* to 4,4′-bis(carboxyvinyl)-2,2′-bipyridine ring and the other is *trans* to NCS ligand. The heterogenity in the pyridyl rings is due to variation in the electron donation from ligand to metal and the back donation from metal to ligand, which is evident up to methyl carbons of the nonyl chains. The difference in the chemical shifts of ($-C_1$) attached on the 4,4′-positions of 2,2-bipyridine is 0.41 ppm that decreases to 0.06 in $-CH_3$ of ($-C_9$).

4.4. FTIR spectra

The ATR-FTIR spectra of the K9 complex show a strong and intense absorption at 2098 cm^{-1} due to the N-coordinated υ(CN). This band is approximately 2.8 times more intense than the band at 804 cm^{-1}, due to υ(CS). The bands at 1698 cm^{-1} and 1226 cm^{-1} are assigned to the υ(C=O) and υ(C–O) stretching of carboxylic acid groups, respectively. The four bands at 1613, 1540, 1473 and 1420 cm^{-1} are due to the ring stretching modes of the ligands. The IR bands at 1635 and 975 cm^{-1} are due to characteristic υ(C=C) and *trans*-υ(C–H), respectively of 4,4′-bis(carboxyvinyl)-2,2′-bipyridine.

The ATR-FTIR data of the K8 and the K9 complexes anchored onto 2 μm thick nanocrystalline TiO_2 films reveal the mode of adsorption of these dyes onto the TiO_2 surface. The ATR-FTIR spectrum of the adsorbed K9 complex shows the presence of carboxylate asymmetric at 1601 $\upsilon(-COO^-_{as})$ and symmetric at 1371 cm^{-1} $\upsilon(-COO^-_{s})$ bands, confirming that the carboxylic acid protons are dissociated and involved in the adsorption on the TiO_2 surface. On the other hand, the adsorbed K8 complex on TiO_2 films shows the presence of carboxylic acid υ(C=O) at 1706 cm^{-1}, and the carboxylate asymmetric $\upsilon(-COO^-_{as})$ at 1634 and symmetric $\upsilon(-COO^-_{s})$ at 1374 cm^{-1} bands indicating that the four carboxylic acid groups are not involved in the adsorption on the TiO_2 surface. In both the complexes, the υ(CN) at 2098 cm^{-1} and the υ(CS) at 804 cm^{-1} bands remained unchanged between the solid and the anchored K8 and K9 complexes.

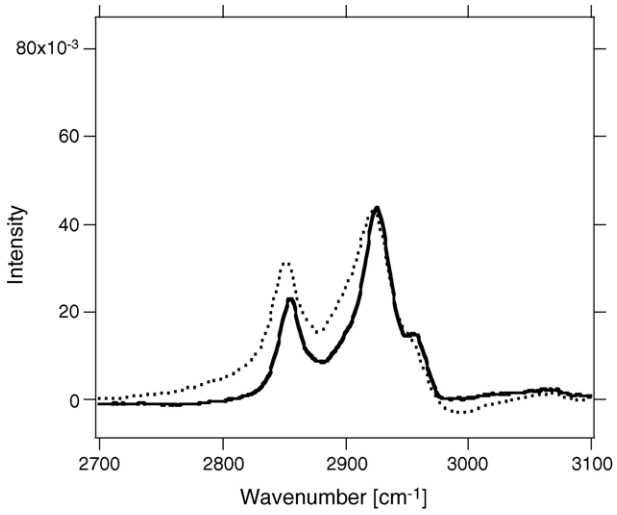

Fig. 5. A portion of the normalized ATR-FTIR spectra of the K9 complex obtained using a solid sample (dotted line) and adsorbed on a 2 μm thick nanocrystalline TiO_2 film (solid line). The intensity of the adsorbed K9 complex is 3.5 times lower than the solid sample.

Fig. 5 presents infrared spectra in the CH_2 stretching mode region of the K9 complex in the solid state and adsorbed onto a TiO_2 film. The position of the CH_2 stretching band in the region between 2849 and 2854 cm^{-1} provides a qualitative measure of the conformational disorder. A higher wave number of this vibrational band is known to reflect a higher conformational disorder [21]. The K9 solid sample show broad bands at 2851, 2922 and 2948 cm^{-1}, which are due the symmetric and antisymmetric $\upsilon(CH_2)$ vibrations of the alkyl chains, respectively [22,23]. The K9 complex adsorbed onto TiO_2 film shows bands at 2855, 2926 and 2956 cm^{-1}, which are shifted to higher energy compared to the bands observed for the solid state K9 sample, revealing a higher conformational disorder of the C_9H_{19} alkyl chains [23]. In addition to a slight increase of disorder for C_9H_{19} alkyl chains, sharper peaks of the adsorbed complex (Fig. 5) indicate a higher chain rigidity. The superior rigidity with a higher chain disorder suggests possible intra and/or inter molecular interactions between the C_9H_{19} groups, resulting in an aliphatic chain net work on the TiO_2 surface. This type of interaction is beneficial for a dye-sensitized solar cell where access to the oxidized redox couple for conduction band electrons is reduced, ensuing an increase in open circuit potential for dye-sensitized solar cell (see Section 4.6).

4.5. Electrochemical data

The electrochemical properties of the K9 complex were scrutinized by cyclic voltammetry in DMF solvent with 0.1 M tetrabutyl ammonium perchlorate using a glassy carbon electrode. The K9 complex shows a couple at 0.25 V versus

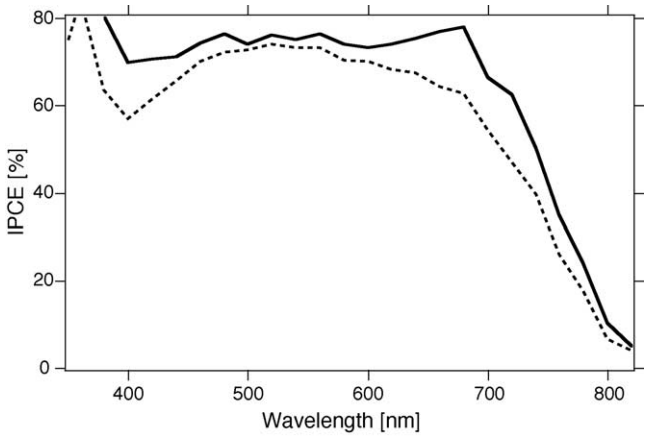

Fig. 6. Photocurrent action spectra obtained with the K8 (solid line) and the K9 (dashed line) complexes attached to nanocrystalline TiO_2 film. The incident photon to current conversion efficiency is plotted as a function of the wavelength of the exciting light. The electrolyte composition was 0.6M M-methyl-*N*-butyl imidazolium iodide, 0.05 M iodine, 0.05 M LiI and 0.5 M *tert*-butylpyridine in a 50:50 (v/v) mixture of valeronitirile and acetonitrile.

Fc^+/Fc with a separation of 0.1 V between anodic and cathodic peak, which is due to $Ru^{III/II}$. When scanning towards negative potentials two reversible waves were observed at $E_{1/2} = -1.98$ and -2.25 versus Fc^+/Fc, which are assigned to the reduction of 4,4′-bis(carboxyvinyl)-2,2′-bipyridine and 4,4′-dinonyl-2,2′-bipyridine, respectively. Under similar conditions the K8 complex exhibits a quasi-reversible oxidation and a reversible reduction potential at $E_{1/2} = 0.35$ and -1.83 V versus Fc^+/Fc, respectively [14]. The cathodic shift in the ruthenium oxidation and the ligand reduction potentials in K9 compared to K8 is due to the presence of 4,4′-dinonyl-2,2′-bipyridine, which is a stronger donor than the 4,4′-bis(carboxyvinyl)-2,2′-bipyridine.

4.6. Photovoltaic data

The photocurrent action spectra of the K8 and K9 sensitizers obtained with the sandwich cell, under illumination, are shown in Fig. 6. The spectra of incident monochromatic photon-to-current conversion efficiency (IPCE), plotted as a function of excitation wavelength show in the plateau region 77% for the K8 sensitizer. Strikingly, the incident monochromatic photon-to-current conversion efficiency is 66% even at 700 nm. From the overlap integral of this curve one measures a short circuit photocurrent density of 18.1 mA/cm^2. In agreement with this measurement, under a standard global air mass 1.5 solar condition, the cell gave a photocurrent density of 18 ± 0.5 mA/cm^2, 640 ± 50 mV open circuit potential and 0.75 fill factor yielding 8.64% efficiency [14].

The K9-sensitized solar cell showed 73% incident photon-to-current conversion efficiency at the plateau region and only 54% efficiency at 700 nm. The IPCE data of the K8 complex show an enhanced red response compared to the K9 complex, which is consistent with the absorption spectra of these two sensitizers in solution and anchored on TiO_2 films. At one sun, the K9-sensitized solar cell gave a photocurrent density of 16.5 ± 0.5 mA/cm^2, 666 ± 50 mV open circuit potential and 0.71 fill factor yielding 7.8% efficiency. The purpose of designing the K9 complex is that structural features of the dye should match the requirements for current rectification in analogy to the photo-field effect in transistors, the gate for unidirectional electron flow from the electrolyte through the junction and into the oxide is opened by the photo-excitation of the sensitizer. The reverse charge flow, i.e. re-capture of the electron by the oxidized redox couple in the electrolyte is impaired by judicious design of the sensitizer having alkyl chains 4,4′-nonyl-2,2′-bipyridine. The latter should form a tightly packed insulating monolayer blocking the dark current. The increase of 26 mV open circuit potential in K9 (666 mV) compared to the K8 (640 mV) sensitizer clearly reflects this point.

Table 1
Performance characteristics of photovoltaic cells based on nanocrystalline TiO_2 films sensitized by K8 from 1:1 CH_3CN and *tert*-butanol solution with different TiO_2 thickness using 1376 electrolyte at one sun

TiO_2 layer thickness (μm)	Current (mA/cm^2)	Potential (mV)	Fill factor	Efficiency
8 + 4	16.9 ± 0.3	665 ± 30	0.73 ± 0.05	8.20
10 + 4	17.7 ± 0.3	645 ± 20	0.74 ± 0.05	8.45
12 + 4	18.0 ± 0.3	640 ± 20	0.75 ± 0.05	8.64
16 + 4	18.0 ± 0.3	638 ± 50	0.72 ± 0.05	8.26

From the photovoltaic data it is apparent that the significant effect asserted by the ligands containing an extended conjugation exhibit enhanced spectral response. The excellent efficiency of the K8 dye-sensitized solar cell of thin TiO_2 films results from its strong optical light absorbance across the visible spectrum and superior response in the red region. Table 1 illustrates the correlation between TiO_2 electrodes thickness and performance characteristics obtained using the K8 sensitizer with the 1376 electrolyte. The table shows that doubling the TiO_2 thickness resulted only in a 6% increase in the short circuit current revealing the advantages of dyes having high molar extinction coefficient. It is striking to note that the insertion of the vinyl moiety in the binding ligand does not reduce the electronic coupling between the dye cation and the TiO_2 electrode, consistent with the unsaturated nature of this moiety. Further improvement in the efficiency of the K8 and the K9 sensitizers is possible by optimizing the number of protons, dye deposition solvent and electrolyte composition. The work directed towards this goal is in progress.

5. Conclusions

We have successfully tuned the HOMO and the LUMO levels of the ruthenium sensitizer that show an enhanced spectral response and an increased molar extinction coefficient yielding a close to 8.7% efficient cell. Our goal of reducing transport losses in the nanoporous environment by increasing the optical extinction coefficient of sensitizers, so that dye

solar cells could be made thinner and thus more efficient, is demonstrated. To our knowledge this class of sensitizers is novel and opens the way to design more efficient panchromatic sensitizers that absorb all the visible light including in the near IR region by further modification of the ligand architecture, which will improve notably power conversion efficiencies of dye-sensitized solar cell.

Acknowledgments

We acknowledge financial support of this work by the Swiss Federal Office for Energy (OFEN), and U.S. Air Force Research Office under contract number F61775-00-C0003. We thank Dr. Robin Humphry-Baker for his time and helpful discussions.

References

[1] M. Grätzel, Nature 414 (2001) 338.
[2] S. Nakade, Y. Saito, W. Kubo, T. Kitamura, Y. Wada, S. Yanagida, J. Phys. Chem. B 107 (2003) 8607.
[3] E. Palomares, J.N. Clifford, S.A. Haque, T. Lutz, J.R. Durrant, J. Am. Ceram. Soc. 125 (2003) 475.
[4] K. Hara, T. Sato, R. Katoh, A. Furube, Y. Ohga, A. Shinpo, S. Suga, K. Sayama, H. Sugihara, H. Arakawa, J. Phys. Chem. B 107 (2003) 597.
[5] K.D. Benkstein, N. Kopidakis, J. van de Lagemaat, A.J. Frank, J. Phys. Chem. B 107 (2003) 7759.
[6] F.L. Qiu, A.C. Fisher, A.B. Walker, L.M. Petecr, Electrochem. Commun. 5 (2003) 711–716.
[7] J. He, G. Benko, F. Korodi, T. Polivka, R. Lomoth, B. Åkermark, L. Sun, A. Hagfeldt, V. Sundstrom, J. Am. Chem. Soc. 124 (2002) 4922.
[8] M.K. Nazeeruddin, A. Kay, I. Rodicio, R. Humphry-Baker, E. Muller, P. Liska, N. Vlachopoulos, M. Grätzel, J. Am. Chem. Soc. 115 (1993) 6382.
[9] M. Yanagida, T. Yamaguchi, M. Kurashige, K. Hara, R. Katoh, H. Sugihara, H. Arakawa, Inorg. Chem. 42 (2003) 7921.
[10] G. Sauvé, M.E. Cass, S.J. Doig, I. Lauermann, K. Pomykal, N.S. Lewis, J. Phys. Chem. 104 (2000) 3488.
[11] R. Argazzi, C.A. Bignozzi, T.A. Heimer, F.N. Castellano, G.J. Meyer, Inorg. Chem. 33 (1994) 5741.
[12] T.A. Heimer, E.J. Heilweil, C.A. Bignozzi, G.J. Meyer, J. Phys. Chem. A 104 (2000) 4256.
[13] P. Dupau, T. Renouard, H.L. Bozec, Tetrahedron Lett. 37 (1996) 7503.
[14] C. Klein, M.K. Nazeeruddin, P. Liska, D. Di Censo, N. Hirata, E. Palomares, J.R. Durrant, M. Grätzel, Inorg. Chem. 44 (2005) 178.
[15] M.K. Nazeeruddin, P. Péchy, T. Renouard, S.M. Zakeeruddin, R. Humphry-Baker, P. Comte, P. Liska, C. Le, E. Costa, V. Shklover, L. Spiccia, G.B. Deacon, C.A. Bignozzi, M. Grätzel, J. Am. Chem. Soc. 123 (2001) 1613.
[16] V. Balzani, A. Juris, M. Venturi, S. Campagna, S. Serroni, Chem. Rev. 96 (1996) 759.
[17] T.J. Meyer, Pure Appl. Chem. 50 (1986) 1293.
[18] P.B. Hitchcock, K.R. Seddon, J.E. Turp, Y.Z. Yousif, J.A. Zora, E.C. Constable, O. Wernberg, J. Chem. Soc. Dalton Trans. (1988) 1837.
[19] M.K. Nazeeruddin, S.M. Zakeeruddin, R. Humphry-Baker, S.I. Gorelsky, A.B.P. Lever, M. Grätzel, Cooed. Chem. Rev. 208 (2000) 213.
[20] M.K. Nazeeruddin, S.M. Zakeeruddin, R. Humphry-Baker, S.I. Gorelsky, A.B.P. Lever, M. Grätzel, Coord. Chem. Rev. 208 (2000) 213.
[21] R.G. Snyder, J. Chem. Phys. 47 (1967) 1316.
[22] K.S. Finnie, J.R. Bartlett, J.L. Woolfrey, Langmuir 14 (1998) 2744.
[23] M.J. Hostetler, J.J. Stokes, R.W. Murray, Langmuir 12 (1996) 3604.